AIAA JOURNAL
Vol. 45, No. 12, December 2007

Systems Identification Approach for a Computational-Fluid-Dynamics-Based Aeroelastic Analysis

K. K. Gupta* and C. Bach†
NASA Dryden Flight Research Center, Edwards, California 93523-0273

DOI: 10.2514/1.28647

This paper presents a novel state-space model-based systems identification method for accurate and efficient simulation of the aeroelastic phenomenon of flight vehicles, among others. Both structural and fluid discretization are achieved by the common finite element method, their interactions being modeled by the transpiration boundary condition technique. The computational fluid dynamics analysis is valid for either inviscid or viscous flow, and structural deformation is assumed to be small in nature. A number of example problems are solved by the systems identification procedure, developed herein, and such results are compared with that obtained by the direct time-marched analysis method reported earlier. The examples include a cantilever wing with a NACA 0012 airfoil, the Hyper X launch vehicle, and the F/A-18 AAW aircraft. These analysis results show a considerable improvement in central processing unit solution time for the new systems identification procedure over the usual time-marched solution.

Nomenclature

$\hat{\mathbf{C}}$	=	generalized damping matrix
$\boldsymbol{f}_a(t)$	=	generalized aerodynamic load vector
$\boldsymbol{f}_I(t)$	=	generalized impulse force vector
$\boldsymbol{f}_i, \boldsymbol{g}_i$	=	flux vector convection and diffusion terms
$\mathbf{G}_a, \mathbf{H}_a, \mathbf{C}_a, \mathbf{D}_a$	=	aerodynamic state-space matrices
$\mathbf{G}_s, \mathbf{H}_s, \mathbf{C}_s, \mathbf{D}_s$	=	structural state-space matrices
$\mathbf{G}_{\text{sa}}, \mathbf{H}_{\text{sa1}}, \mathbf{H}_{\text{sa2}}$	=	aeroelastic state-space matrices
$\hat{\mathbf{K}}$	=	generalized stiffness matrix
$\hat{\mathbf{M}}$	=	generalized mass matrix
$\boldsymbol{q}$	=	generalized displacement vector
t, T	=	time and temperature
$\boldsymbol{u}$	=	displacement vector
v	=	volume
ρ	=	freestream density
$\hat{\rho}$	=	training density for the auto regressive moving average model

Introduction

MANY practical problems, such as flight vehicles [1,2], are characterized by unprecedented interactions among a number of major disciplines as fluids, structures, thermal, propulsion, and controls, among others. Furthermore, in some critical flight regimes like transonic flow, the dynamic behavior of fluids becomes highly complicated and linear aerodynamic methods become unreliable for prediction of unsteady flow. It is then necessary to employ computational-fluid-dynamics-based (CFD-based) simulations for an accurate assessment of multidisciplinary interactions such as the aeroelastic and aeroservoelastic phenomenon. In particular, vehicles with complex geometry require such a simulation to be able to derive meaningful and reliable results.

Some past efforts [3–6] in this direction have been made in which the finite difference or finite volume methods are adopted for fluid flow, which are then coupled with the structural vibration data derived from finite element models. Recent efforts involving seamless coupling of the finite element based fluids [7,8] and structural data have shown promising results [9,10], which were verified with wind-tunnel as well as flight test data. To determine the onset of aeroelastic instability within a specified flight envelope, it is essential to perform such an analysis for a number of chosen flight conditions. Thus, corresponding to a flight Mach number, evaluations need to be made at a number of altitudes identified by various density values. Whereas such analyses yield accurate solutions, it also requires rather high computer CPU time, making the process rather expensive and time consuming; such an effort involving both aeroelasticity (AE) and aeroservoelasticity (ASE) analyses is depicted in [11]. This paper presents a new, alternative, and much more economical systems identification technique for accurate aeroelastic analysis of complex, practical problems such as aircraft and other flight vehicles. Description of this autoregressive moving average (ARMA) model is provided in broad details followed by a number of relevant example problems, such as a cantilever wing, the Hyper X launch vehicle and the F/A-18 AAW aircraft, along with experimental test correlation whenever available. These results, along with computational CPU times, are then compared with that obtained by the direct time-marched method, which demonstrates considerable advantage of the present systems integration (SI) procedure over the usual time-marched (TM) analysis-based solutions.

Aeroelastic State-Space Matrix Formulation

In this analysis, both the fluid and solid domains are idealized by the common finite element method. This procedure starts with the finite element structural modeling and subsequently computes the natural frequencies ω and modes $\boldsymbol{\phi}$, incorporating rigid-body, elastic, and control surface motions by solving

$$\mathbf{M}\ddot{\boldsymbol{u}} + \mathbf{K}\boldsymbol{u} = \mathbf{0} \tag{1}$$

in which $\mathbf{M}$ and $\mathbf{K}$ are the inertial and stiffness matrices, respectively, and $\boldsymbol{u}$ is the displacement vector. A steady-state Euler/Navier–Stokes solution is effected next, using the local time-stepping, two-step solution procedure described earlier [11–13]. Associated vehicle equation of motion is then cast into the frequency domain

$$\hat{\mathbf{M}}\ddot{\boldsymbol{q}} + \hat{\mathbf{C}}\dot{\boldsymbol{q}} + \hat{\mathbf{K}}\boldsymbol{q} + \boldsymbol{f}_a(t) + \boldsymbol{f}_I(t) = 0 \tag{2}$$

in which $\boldsymbol{q}$ is the displacement vector ($=\boldsymbol{\phi}^T\boldsymbol{u}$); $\hat{\mathbf{M}}$ is the generalized inertia matrix ($=\boldsymbol{\phi}^T\mathbf{M}\boldsymbol{\phi}$), and, similarly, $\hat{\mathbf{K}}$, $\hat{\mathbf{C}}$ the stiffness and damping matrices; $\boldsymbol{f}_a(t)$ is the generalized aerodynamic (CFD) load vector ($=\boldsymbol{\phi}_a^T pA$), p is the fluid pressure at a fluid node, and A is the appropriate surface area around the node; $\boldsymbol{\phi}_a$ is the modal vector at

Received 31 October 2006; revision received 6 June 2007; accepted for publication 25 July 2007.

*Staff, Research Engineering Directorate. Associate Fellow AIAA.
†Senior Engineer, Analytical Services and Materials, Inc.

aerodynamic grid points interpolated from relevant structural modes and $\boldsymbol{f}_l(t)$ is the applied generalized structural impulse force vector.

A state-space matrix equation form of Eq. (2) is written as

$$\begin{bmatrix} \mathbf{I} & 0 \\ 0 & \mathbf{I} \end{bmatrix} \begin{bmatrix} \dot{\boldsymbol{q}} \\ \ddot{\boldsymbol{q}} \end{bmatrix} - \begin{bmatrix} 0 & \mathbf{I} \\ -\hat{\mathbf{M}}^{-1}\hat{\mathbf{K}} & -\hat{\mathbf{M}}^{-1}\hat{\mathbf{C}} \end{bmatrix} \begin{bmatrix} \boldsymbol{q} \\ \dot{\boldsymbol{q}} \end{bmatrix} - \begin{bmatrix} 0 \\ -\hat{\mathbf{M}}^{-1}\boldsymbol{f}_a(t) \end{bmatrix} - \begin{bmatrix} 0 \\ -\hat{\mathbf{M}}^{-1}\boldsymbol{f}_l(t) \end{bmatrix} = 0 \tag{3}$$

or

$$\dot{\mathbf{x}}_s(t) = \mathbf{A}_{\mathrm{st}}\mathbf{x}_s(t) + \mathbf{B}_{\mathrm{st}}\boldsymbol{f}(t) \tag{4}$$

where

$$\mathbf{B}_{\mathrm{st}} = \begin{bmatrix} 0 \\ -\hat{\mathbf{M}}^{-1} \end{bmatrix}, \qquad \boldsymbol{f}(t) = \boldsymbol{f}_a(t) + \boldsymbol{f}_l(t), \qquad \mathbf{x}_s(t) = \begin{bmatrix} \boldsymbol{q} \\ \dot{\boldsymbol{q}} \end{bmatrix} \tag{5}$$

and

$$\mathbf{y}_s(t) = \mathbf{C}_{\mathrm{st}}\mathbf{x}_s(t) + \mathbf{D}_{\mathrm{st}}\boldsymbol{f}(t) \tag{6}$$

in which $\mathbf{C}_{\mathrm{st}} = \mathbf{I}$ and $\mathbf{D}_{\mathrm{st}} = 0$. These equations are then converted to the zero-order hold (ZOH) discrete time equivalent at the kth step:

$$\mathbf{x}_s(k+1) = \mathbf{G}_s\mathbf{x}_s(k) + \mathbf{H}_s\boldsymbol{f}(k) \tag{7}$$

$$\mathbf{y}_s(k) = \mathbf{C}_s\mathbf{x}_s(k) + \mathbf{D}_s\boldsymbol{f}(k) \tag{8}$$

where

$$\mathbf{G}_s = e^{\mathbf{A}_s\Delta t}, \quad \text{and} \quad \mathbf{H}_s(k) = [e^{\mathbf{A}_s\Delta t} - \mathbf{I}][\mathbf{A}_s^{-1}\mathbf{B}_s] \tag{9}$$

$$\boldsymbol{f}(k) = \boldsymbol{f}_a(k) + \boldsymbol{f}_l(k) \tag{10}$$

and $\Delta t = t_{k+1} - t_k$, $\mathbf{C}_s$, and $\mathbf{D}_s$ remain unchanged.

State-Space Systems Identification Model in Aeroelastic Analysis

The system identification technique model structure used herein is the autoregressive moving average model (ARMA). In this process, the modal response force at time k of a system is taken as a summation of scaled previous outputs and scaled values of modal displacement inputs to the system. This model makes the assumptions that most aeroelastic systems can be treated as dynamically linear and that the aerodynamics respond linearly to small perturbations about a potential nonlinear steady-state mean flow. A basic ARMA model in Fig. 1 at time k may be written as

$$\boldsymbol{f}_a(k) = \sum_{i=1}^{na} \boldsymbol{A}_i\boldsymbol{f}_a(k-i) + \frac{1}{\hat{\rho}}\sum_{i=0}^{nb-1} \boldsymbol{B}_i\boldsymbol{q}(k-i) \tag{11}$$

where $\boldsymbol{A}_i$ and $\boldsymbol{B}_i$ are unknowns to be determined from excitation of the structure through a prescribed motion containing the spectrum of calculated structural eigenmodes, and na and nb are the orders of the coefficient of $\boldsymbol{A}$s and $\boldsymbol{B}$s. The training density $\hat{\rho}$ may be used to scale

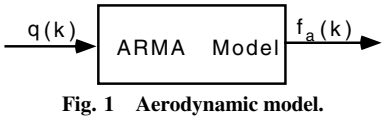

Fig. 1 Aerodynamic model.

the generalized force and that further scaling the generalized forces on the right-hand side results in

$$\hat{\boldsymbol{f}}_a(k) = \sum_{i=1}^{na} \boldsymbol{A}_i\hat{\boldsymbol{f}}_a(k-i) + \frac{1}{\hat{\rho}}\sum_{i=0}^{nb-1} \boldsymbol{B}_i\boldsymbol{q}(k-i) \tag{12}$$

A state vector $\boldsymbol{x}_a$ is next defined for the scaled aerodynamic system which contains a total of $(na + nb - 1)$ number of roots states

$$\boldsymbol{x}_a(k) = \begin{bmatrix} \hat{\boldsymbol{f}}_a(k-1) \\ \vdots \\ \hat{\boldsymbol{f}}_a(k-1) \\ \boldsymbol{q}(k) \\ \vdots \\ \boldsymbol{q}(k-nb+1) \end{bmatrix} \tag{13}$$

Based on any given structural displacement inputs, the mathematical model of the unsteady CFD aerodynamic system can compute the aerodynamic forces outputs. Therefore, the mathematical state-space representation of the aerodynamic system can replace the traditional Euler/N-S CFD step in the multidisciplinary aeroelastic or aeroservoelastic analysis.

The state-space form for the scaled aerodynamic model can then be written as

$$\boldsymbol{x}_a(k+1) = \mathbf{G}_a\boldsymbol{x}_a(k) + \mathbf{H}_a\boldsymbol{q}(k) \tag{14}$$

$$\hat{\boldsymbol{f}}_a(k) = \mathbf{C}_a\boldsymbol{x}_a(k) + \mathbf{D}_a\boldsymbol{q}(k) + \hat{\boldsymbol{f}}_{\mathbf{0}} \tag{15}$$

in which

$$\begin{bmatrix} \mathbf{A_1} & \mathbf{A_2} & \cdots & \mathbf{A}_{na-1} & \mathbf{A}_{na} & \frac{1}{\hat{\rho}}\mathbf{B}_1 & \frac{1}{\hat{\rho}}\mathbf{B}_2 & \cdots & \frac{1}{\hat{\rho}}\mathbf{B}_{nb-2} & \frac{1}{\hat{\rho}}\mathbf{B}_{nb-1} \\ \mathbf{I} & 0 & \cdots & 0 & 0 & 0 & 0 & \cdots & 0 & 0 \\ 0 & \mathbf{I} & & 0 & 0 & 0 & 0 & \cdots & 0 & 0 \\ \vdots & \vdots & & \vdots & \vdots & \vdots & \vdots & \ddots & \vdots & \vdots \\ 0 & 0 & & \mathbf{I} & 0 & 0 & 0 & \cdots & 0 & 0 \\ 0 & 0 & & 0 & 0 & 0 & 0 & \cdots & 0 & 0 \\ 0 & 0 & & 0 & 0 & \mathbf{I} & 0 & \cdots & 0 & 0 \\ 0 & 0 & & 0 & 0 & 0 & \mathbf{I} & \cdots & 0 & 0 \\ \vdots & \vdots & & \vdots & \vdots & \vdots & \vdots & \ddots & \vdots & \vdots \\ 0 & 0 & & 0 & 0 & 0 & 0 & \ldots & \mathbf{I} & 0 \end{bmatrix}$$

$$\mathbf{H}_a = \begin{bmatrix} \frac{1}{\hat{\rho}}\mathbf{B}_0 \\ 0 \\ 0 \\ \vdots \\ 0 \\ \mathbf{I} \\ 0 \\ 0 \\ \vdots \\ 0 \end{bmatrix}$$

$$\mathbf{C_a} = \begin{bmatrix} \mathbf{A}_1 & \mathbf{A}_2 & \cdots & \mathbf{A}_{na-1} & \mathbf{A}_{na} & \frac{1}{\hat{\rho}}\mathbf{B}_1 & \frac{1}{\hat{\rho}}\mathbf{B}_2 & \cdots & \frac{1}{\hat{\rho}}\mathbf{B}_{nb-2} & \frac{1}{\hat{\rho}}\mathbf{B}_{nb-1} \end{bmatrix}$$

$$\mathbf{D}_a = \frac{1}{\hat{\rho}}\mathbf{B}_o, \qquad \boldsymbol{q}(k) = \boldsymbol{T}_a\mathbf{y}_s(k) = [\mathbf{I} \;\; 0]\mathbf{y}_s(k) \tag{16}$$

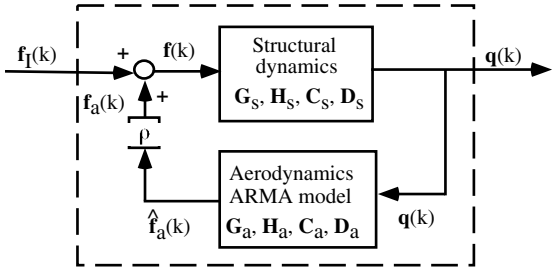

Fig. 2 Coupled ARMA aeroelastic model.

The output equation for the scaled aerodynamic model may include a known vector of static offset $\hat{f}_0 = f_0/\hat{\rho}$ which are subtracted off of the time history data in the derivation of the aerodynamic model, because the ARMA model structure only models the dynamics of the system. The generalized force vector $f_a(=\rho\hat{f}_a)$ is then fed back into structural state-space matrix Eqs. (7) and (8) in the solution iteration as shown in Fig. 2. The matrices **A** and **B** are of dimension $NR \times NR$. Further details of model identification and input optimization are given in [12].

Autoregressive Moving Average Model Aeroelastic Analysis

A combined structural and aerodynamic state-space matrix formulation is derived next for the coupled aeroelastic model, which enables depiction of aeroelastic root-locus plots which assists in the control law design. Thus, the aerodynamic state-space equation's input can be written in terms of the structural output as follows

$$\boldsymbol{x}_a(k+1) = \mathbf{G}_a\boldsymbol{x}_a(k) + \mathbf{H}_a\mathbf{T}_a\mathbf{C}_s\mathbf{x}_s(k) \tag{17}$$

$$\boldsymbol{f}_a(k) = \rho\mathbf{C}_a\boldsymbol{x}_a(k) + \rho\mathbf{D}_a\mathbf{T}_a\mathbf{C}_s\mathbf{x}_s(k) + \rho\hat{\boldsymbol{f}}_a \tag{18}$$

and $\boldsymbol{f}_a$ can be obtained as

$$\boldsymbol{f}_a(k) = \boldsymbol{f}_I(k) + \boldsymbol{f}_a(k) \tag{19}$$

Substitution of Eqs. (17) and (18) into Eqs. (7) and (8) yields

$$\mathbf{x}_s(k+1) = (\mathbf{G}_s + \mathbf{H}_s\rho\mathbf{D}_a\mathbf{T}_a\mathbf{C}_s)\mathbf{x}_s(k) + \mathbf{H}_s\rho\mathbf{C}_a\boldsymbol{x}_a(k)\mathbf{H}_s\boldsymbol{f}_I + \mathbf{H}_s\rho\hat{\boldsymbol{f}}_a \tag{20}$$

$$\mathbf{y}_s(k) = \begin{Bmatrix}\boldsymbol{q}(k)\\ \dot{\boldsymbol{q}}(k)\end{Bmatrix} = \mathbf{C}_s\mathbf{x}_s(k) \tag{21}$$

and the aeroelastic state-space matrix equation may then be written as

$$\begin{Bmatrix}\mathbf{x}_s(k+1)\\ \boldsymbol{x}_a(k+1)\end{Bmatrix} = \begin{bmatrix}\mathbf{G}_s + \rho\mathbf{H}_s\mathbf{D}_a\mathbf{T}_a\mathbf{C}_s & \rho\mathbf{H}_s\mathbf{C}_a\\ \mathbf{H}_a\mathbf{T}_a\mathbf{C}_s & \mathbf{G}_a\end{bmatrix}\begin{Bmatrix}\mathbf{x}_s(k)\\ \boldsymbol{x}_a(k)\end{Bmatrix} + \begin{bmatrix}\mathbf{H}_s\\ 0\end{bmatrix}\boldsymbol{f}_I(k) + \begin{bmatrix}\rho\mathbf{H}_s f_0\\ 0\end{bmatrix} \tag{22}$$

$$\begin{bmatrix}\boldsymbol{q}(k)\\ \dot{\boldsymbol{q}}(k)\end{bmatrix} = [\mathbf{C}_s \quad 0]\begin{Bmatrix}\mathbf{x}_s(k)\\ \boldsymbol{x}_a(k)\end{Bmatrix} \tag{23}$$

or

$$\mathbf{x}_{sa}(k+1) = \mathbf{G}_{sa}\mathbf{x}_{sa}(k) + \mathbf{H}_{sa1}\boldsymbol{f}_I(k) + \mathbf{H}_{sa2} \tag{24}$$

$$\mathbf{y}_{sa}(k) = \mathbf{G}_{sa}\mathbf{x}_{sa}(k) \tag{25}$$

The relevant root-locus plot, derived from the $\mathbf{G}_{sa}$ matrix, shows the location of roots as a function of density, which is analog to the plotting of $\boldsymbol{q}$ and $\dot{\boldsymbol{q}}$ contained in $\mathbf{y}_s$ [Eq. (6)]; a requirement of stability dictates that all roots lie within the unit circle. The matrix $\mathbf{G}_{sa}$ can be used for control law design to yield the gain matrix $\tilde{\mathbf{k}}$, which can next be used to plot response of the controlled vehicle.

Following the technique for the direct solution described earlier [11,12], this procedure can be similarly extended for the ASE analysis. The computer flowchart for the ARMA AE/ASE analysis is shown in Fig. 3. Once the structural modal analysis has been performed, the relevant AE/ARMA solution analysis steps can be described as follows:

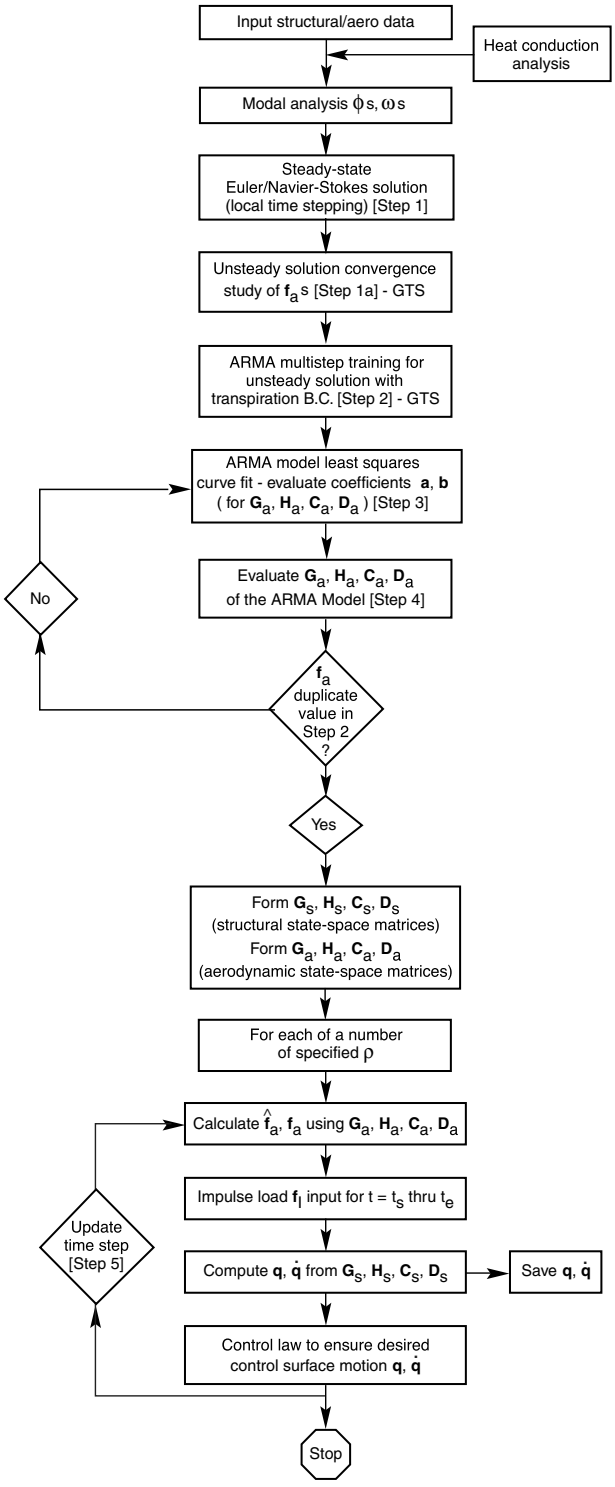

Fig. 3 AE and ASE analysis using ARMA methodology.

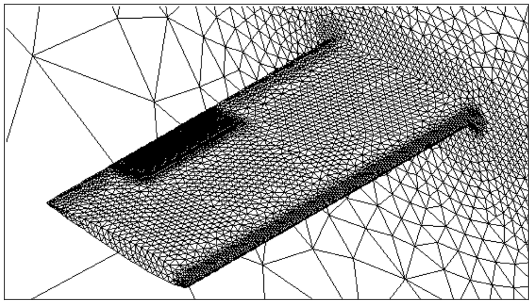

a) aerodynamic model of the wing

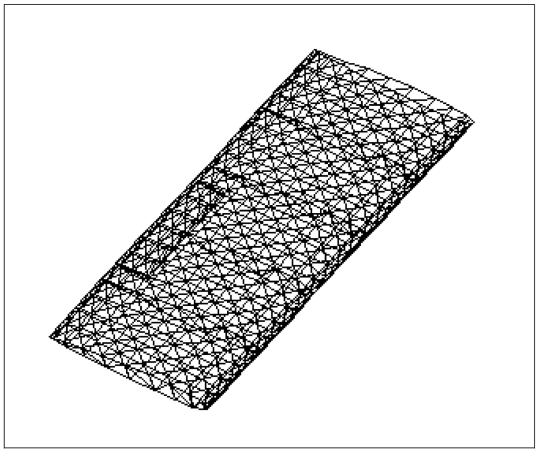

b) FE structural mesh of the wing

Fig. 4 Aerodynamic and structural surface grid of wing and solution domain.

Step 1: Steady-state CFD solution followed by input data preparation for subsequent unsteady analysis.

Step 1a: Unsteady solution convergence study of the clamped structure with sufficient number of solution steps to ensure that the generalized forces form a straight line, each without oscillations.

Step 2: Training the ARMA multistep unsteady solution, employing a transpiration [14,15] boundary condition strategy, for a 3211 or a variable amplitude 753211 input signal for a number of suitable time steps to ensure convergence of solutions $\boldsymbol{q}$ and $\dot{\boldsymbol{q}}$ to their steady states.

Step 3: Least-squares curve fitting for the ARMA model.

Step 4: Evaluation of ARMA model involving comparison of generalized forces obtained in step 1a with that from step 4. If needed, repeat steps 3 and 4 with different combinations of na and nb until the signal $\boldsymbol{f}_a$s match with each other.

Step 5: To conduct ARMA solution and derive damping of the signal for the density under consideration. Repeat step 5 similarly for a series of density values to obtain the density signifying aeroelastic instability that pertains to a zero damping value.

Typically, step 5 computations involving six density values are adequate to ascertain the threshold of instability.

Numerical Examples

A number of relevant ARMA-based aeroelastic problems have been solved to assess the accuracy of the currently developed numerical formulation and the associated software. Some examples of representative test problems are given next. All calculations were performed using a single CPU 3.2 GHz PC, employing the Euler equation and the STARS [16] (structural analysis routines) code.

Example 1: Cantilever Wing with a NACA 0012 Airfoil

Figure 4 shows the finite element (FE) aerodynamic surface grid and solution domain as well as the structural surface grid of the wing with a span to chord length ratio of 2.0. Relevant modeling details are as follows:

Important data parameters:
wingspan = 2.0178
wing chord length = 1.0089
Mach number = 2.0
angle of attack = 0 deg
speed of sound at infinity = 340.29
Structural data
Young's modulus = 6.8947E + 10
Poisson's ratio = 0.3
density = 2764.925
Finite element CFD and structures models data:
number of fluid nodes = 65, 745
number of fluid elements = 351, 932
number of structural nodes = 486
number of structural elements = 1549

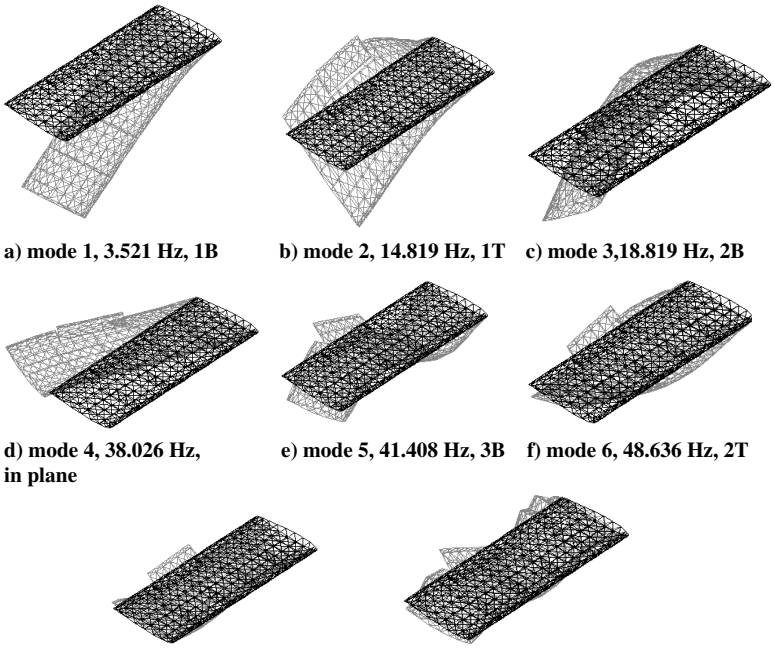

a) mode 1, 3.521 Hz, 1B **b) mode 2, 14.819 Hz, 1T** **c) mode 3,18.819 Hz, 2B**

d) mode 4, 38.026 Hz, in plane **e) mode 5, 41.408 Hz, 3B** **f) mode 6, 48.636 Hz, 2T**

g) mode 7, 59.797 Hz, 1B control **h) mode 8, 64.958 Hz, 4B**

Fig. 5 Structural modes of a cantilever wing.

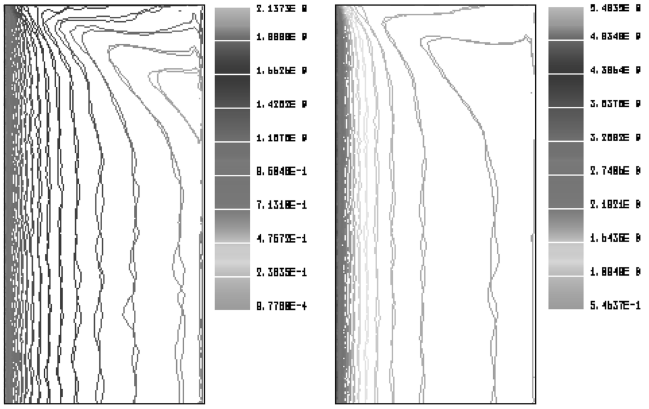

Fig. 6 Cantilever wing steady-state Mach and pressure distribution.

Initial analyses involved aeroelastic and aeroservoelastic simulation [16] for Mach 2.0 using the TM solution method. This is achieved by performing an individual set of analysis, each pertaining to a combination of airspeed and atmospheric density. Next, an ARMA analysis was conducted that employs only one representative unsteady solution, with subsequent training of the same and followed by least-squares curve fitting, evaluation of the ARMA model, and finally conducting the ARMA solution at different input altitudes.

Figure 5 shows a few structural mode shapes pertaining to the various natural frequencies. Results of steady-state CFD analysis performed for Mach 2.0 and density 0.915, in the form of Mach and pressure distribution, are depicted in Fig. 6.

For AE analysis, an unsteady solution is derived and the damping values are calculated from the generalized displacement distributions. Such a distribution of $\boldsymbol{q}$ for a density of 0.915, pertaining to a typical mode 2, is shown in Fig. 7a exhibiting instability; Fig. 7b shows an augmented [16] stable solution with application of control surface motion at time 1 s. Modes 1, 2, and 7 are used for all AE/ASE analyses. These analyses were performed using the direct TM procedure.

An ARMA analysis was then implemented for Mach 2.0 and a training density of 0.915, performing steps 1–4 as described earlier. On satisfactory completion of these analysis steps, ARMA solution of step 5 was achieved pertaining to a number of density values to bracket the flutter point, and Fig. 8 presents the damping plot for the solution domain; the flutter parameter (density ratio) corresponding to the zero damping value is found to be 0.895. Solution time for an unsteady analysis, using the TM method, was found to be about 19 h of CPU time for a typical density value, requiring about 800 solution steps. For the associated ARMA solution, step 1a required 201 steps (CPU = 4 h, 28 min), and step 2 needed 401 steps (CPU = 8 h, 52 min), whereas steps 3–5 required about 26 s for each density value. About six data points are needed to bracket a flutter point and the ARMA solution required 13 h, 21 min to achieve the same; in contrast, the TM solutions needed a total of 114 h of CPU time and, as such, the ARMA procedure proves to be faster than the TM solution by a factor of eight or so.

Example 2: Hypersonic Flight Vehicle (Hyper X)

The Hyper X stack consists of a Pegasus booster and the X-43 hypersonic flight test vehicle. In recently conducted tests, the stack was launched from a B-52 aircraft around an altitude of 22,500 ft and boosted to about 100,000 ft for a Mach 7 and a subsequent Mach 10 flight of the X-43 equipped with a scramjet air breathing engine. Time-marched analyses of the stack [17] and also the X-43 [2] has been reported earlier. An ARMA-based AE analysis of the Hyper X is described next in some detail.

Figure 9 depicts finite element structural (10,000 nodes; 22,000 elements) and CFD (445,000 nodes, 2,650,000 elements) models [11,12] of the stack; Table 1 provides a list of elastic modes considered for the AE analysis. The ARMA analysis was performed for Mach 0.9 and a training density corresponding to an altitude of 22,500 ft; Table 2 presents a comparison of flight measured pressure values to that obtained by the CFD analysis, showing good correlation for the significant data. Solution steps 1, 1a, and 2–4 were routinely conducted to yield a satisfactory ARMA model and, thereafter, step 5 ARMA analyses were performed for a number of desired densities to establish the threshold of aeroelastic instability; the resulting model was found to be highly stable for a wide range of altitudes. Typical generalized displacements $\boldsymbol{q}$ pertaining to the sea

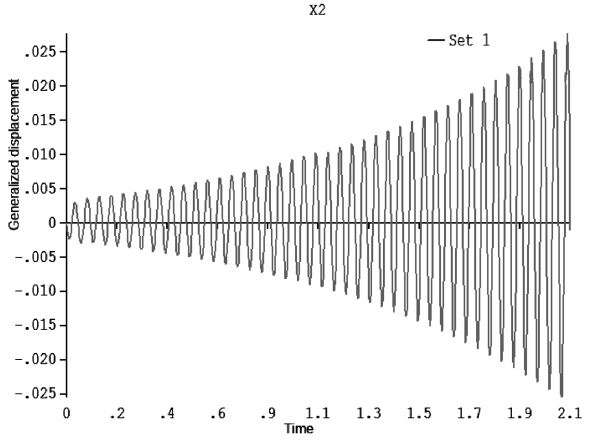

a) AE response

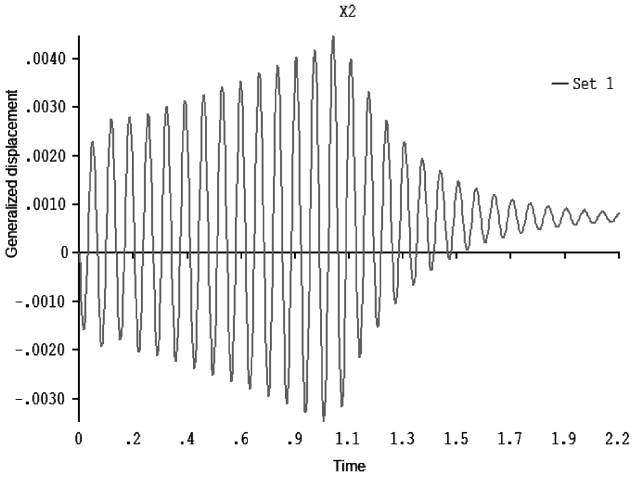

b) ASE response

Fig. 7 Wing AE/ASE response for mode 2.

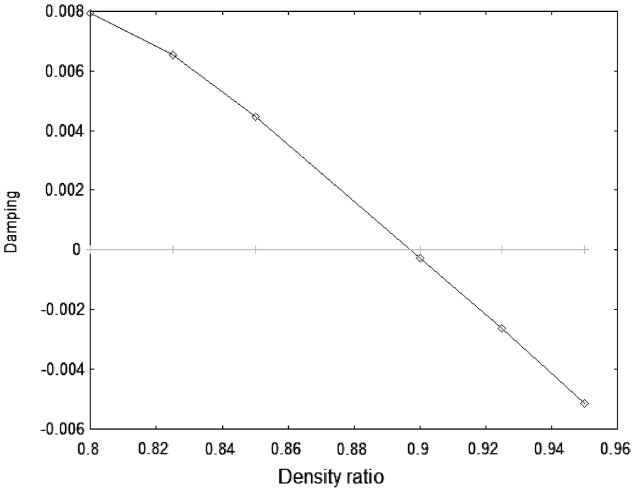

Fig. 8 Aeroelastic ARMA stability plot for cantilever wing for mode 2.

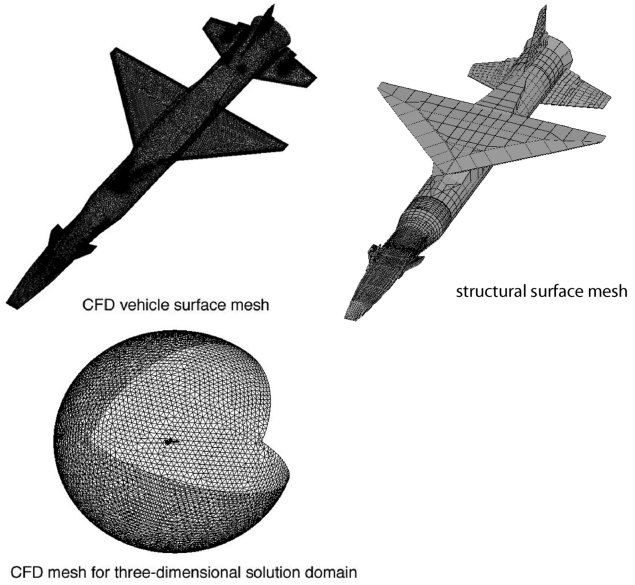

Fig. 9 Hyper X finite element structural and CFD models.

Table 1 Hyper X stack free-vibration analysis results ($\alpha_V = 12.43^0$, $\alpha_{HT} = -11^0$)

Mode	STARS Freq., Hz	Mode shape description (major motion)
1	8.03	F1B vertical (S)
2	9.44	F1B lateral (A/S)
3	13.21	RT fin 1B
4	14.20	rudder 1B
5	14.45	LT fin 1/B
6	16.38	F2B vertical (s)
7	28.97	rudder 1/T

Table 2 Comparison of computed and flight test measured pressure data for the Hyper X

	Pressure, psi	
Sensor point	Flight test	CFD computed
001	1.6900	1.7297
003	1.7800	1.6890
007	−0.2419	−0.1400
085	−0.1567	−0.3886
090	0.078	−0.08

level altitude are shown in Fig. 10. Solution CPU times were 47 h, 12 min for step 1a (200 steps), 106 h for step 2 (450 steps), and about 1 min for steps 3,4, and 5. The TM unsteady solution for a single altitude was 96.8 h, needing 410 solution steps. Assuming that a minimum of six data points are needed for interpolating the instability density, characterized by the zero damping value, it is apparent that the ARMA solution is about four times faster than the corresponding TM analyses; steady solution time is the same for both cases, needing only about 14 h of CPU time.

Example 3: F/A-18 Active Aeroelastic Wing

The Active Aeroelastic Wing (AAW) [18,19] technology program involves a multidisciplinary, aerostructural-controls interactions study that maximizes the performance of a flight vehicle. In this process, a more flexible, lighter wing is used which provides wing twist response at higher speeds and deforms aeroelastically into favorable shapes for optimum performance producing control forces. The primary goal of this program is to generate control laws that will maximize the vehicle performance taking into account wing flexibility. An AE analysis, based on the ARMA technology, was performed on this aircraft, details of which are given next.

Figure 11 depicts the aircraft CFD mesh used for the analysis; the three-dimensional mesh consists of 3,729,316 tetrahedron elements with 672,341 nodes. As the first step of the current analysis, a steady-state CFD solution was achieved, some typical results of which are

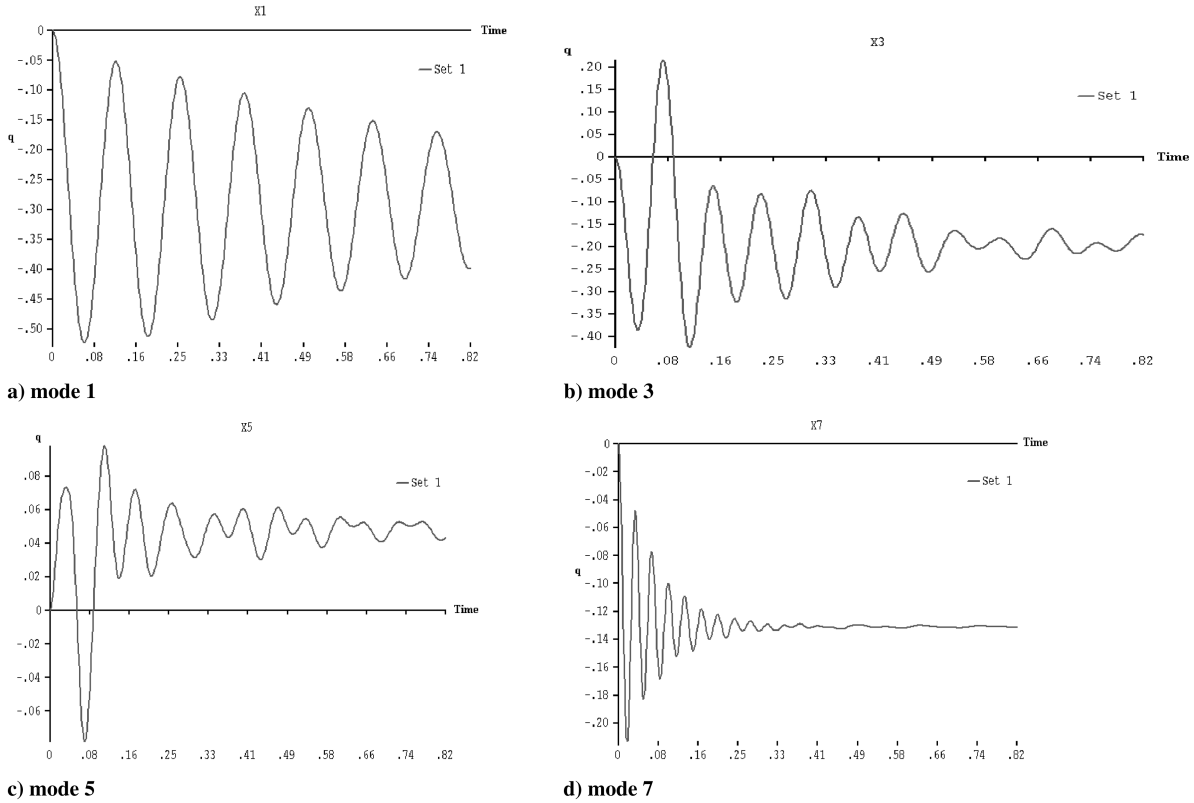

a) mode 1 **b) mode 3**

c) mode 5 **d) mode 7**

Fig. 10 Typical aeroelastic generalized displacements.

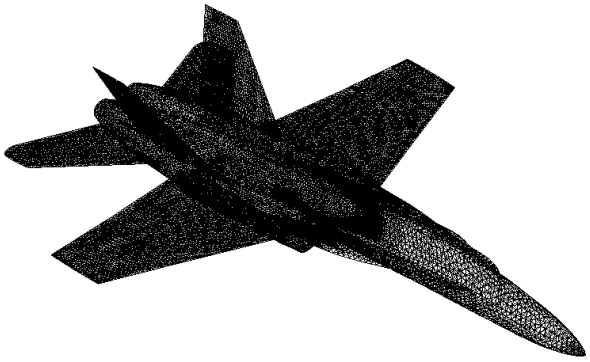

a) Vehicle surface grid

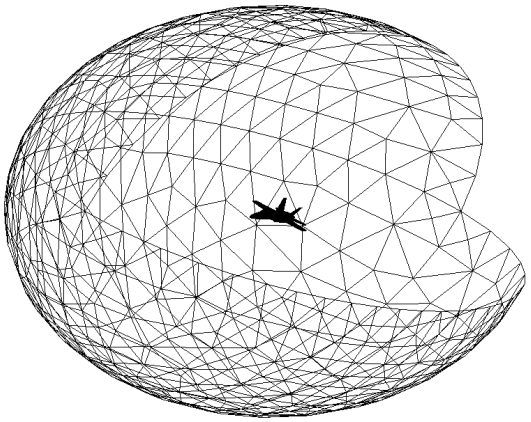

b) Solution domain surface grid

Fig. 11 F/A-18 AAW CFD model.

a) Mach distribution - top view

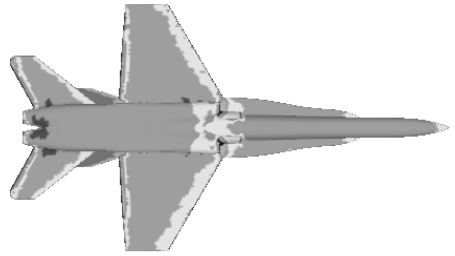

b) Mach distribution - bottom view

c) Mach distribution - cut plane

Fig. 12 Mach distribution on F/A-18 AAW at Mach 0.85.

depicted in Fig. 12. A reduced-order FE structural model of the vehicle was also analyzed to yield the natural frequencies and mode shapes, and Table 3 summarizes the relevant results. An ARMA AE solution was effected for Mach 0.85 for a number of representative altitudes in an effort to determine the stability characteristics and the flutter density corresponding to zero damping value. Distribution of representative generalized displacements for a typical mode (W1B-S) at a number of altitudes are depicted in Fig. 13, showing solution convergence and also divergence pattern. ARMA AE stability plots for the solution domain for Mach 0.85 are shown in Fig. 14; a flutter altitude corresponds to a zero damping value.

A steady-state CFD analysis involving 1000 steps required 2 h, 40 min of CPU time. ARMA solution CPU times were 150 h for step 1a (450 steps), 230 h for step 2 (700 steps), and about 1 min, 30 s for steps 3, 4, and 5. The direct TM solution for each altitude takes 667 h of CPU time, requiring 2000 solution steps. Assuming that around 4–6 data points are needed to determine the flutter altitude, the ARMA procedure proves to be about five times faster than its TM counterpart.

Conclusions

This paper presents details of a novel finite element, CFD-based aeroelastic analysis procedure suitable for efficient modeling and simulation of large complex practical problems. The systems identification procedure employing a new ARMA solution methodology is described herein in some detail. Meshing for CFD idealization is achieved with unstructured grids, which is also standard for structural discretization.

Numerical examples include a cantilever wing with NACA 0012 airfoil and the current solutions are compared with earlier ones using the direct TM method. The second example involves ARMA-based aeroelastic analysis of the Hyper X launch vehicle and such results

Table 3 STARS Free-Vibration Analysis vs GVT F-18 active aeroelastic wing: full model, full fuel[a]

Mode no.	STARS Freq., Hz	GVT, burst Freq., Hz	Mode shape description
1–6	0.0	——	rigid-body modes
7	5.97	6.2	W1B-S, some inboard aileron rotation
8	8.85	8.33	F1B-A, W1B-A
9	9.00	8.69	W1B-A, aft fuse rotation, slight F1B-A
10	9.34	9.87	F1B-S, S1B-S, some wing tip twist
11	13.54	13.01	S1B-A, slight W1T-A
12	13.61	13.49	S1B-S, slight W1T-S
13	14.10	14.53	W1T-S, some S1B-S
14	14.16	15.63	W1T-A, some S1B-A, V1B-A
15	15.71	15.82	V1B-A, some W1T-A, (SF/A-A)
16	15.92	16.28	V1B-S, slight W1T-S, (SF/A-S)

[a]Heavy fuel, weight = 34, 920 lbs; includes modification to wing stiffness after static analysis (Nov. 2001)

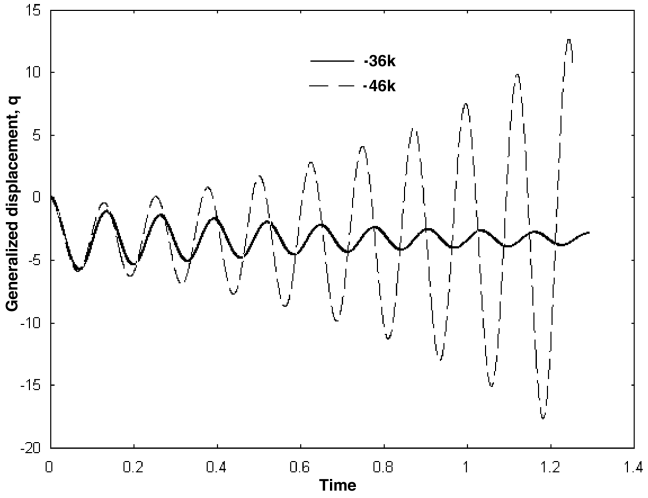

Fig. 13 Typical generalized displacements for mode W1B-S.

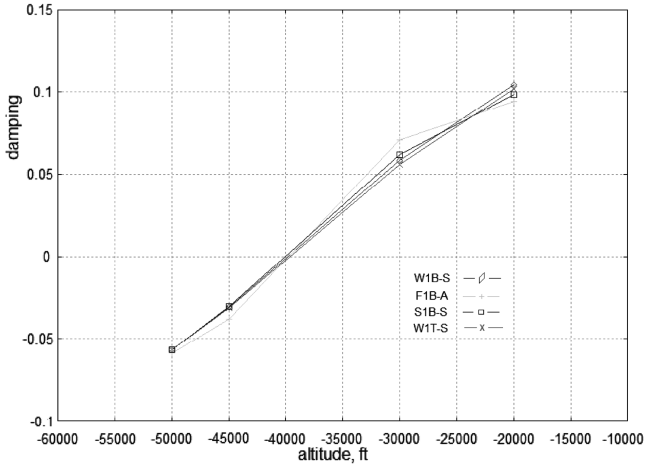

Fig. 14 F/A-18 AAW ARMA/AE instability plots for Mach 0.85.

are further compared with the corresponding TM solutions. Also presented is a comparison of computed pressure values with flight test data. The final example relates to the F/A-18 AAW aircraft and details of the analysis results involving structural, CFD, and ARMA aeroelastic solutions are presented in the paper.

In all of the preceding three example problems, the ARMA solution proves to be much faster than the direct TM method by a factor of 4–10. Such a savings in computer CPU time will enable modest computing resources to yield meaningful solutions pertaining to very large practical problems with complex geometry.

A CFD-based analysis is essential for accurate prediction of unsteady aerodynamics around a complex flight vehicle, particularly in transonic flight regime, where linear panel methods are likely to prove inadequate. Typically, such an analysis demands large computing resources. The ARMA procedure described in this paper will prove to be economical in this regard. State-of-the-art detailed review of the subject matter can be found in [20,21].

Acknowledgments

Thanks are due to S. Lung, A. Arena, E. Hahn, and T. Doyle for their sincere help in the preparation of this work.

References

[1] Ko, W. L., and Gong, L., "Thermostructural Analysis of Unconventional Wing Structures of a Hyper-X Hypersonic Flight Research Vehicle for the Mach 7 Mission," NASA TP-2001-210398, 2001.

[2] Gupta, K. K., Voelker, L. S., Bach, C., Doyle, T., and Hahn, E., "CFD Based Aeroelastic Analysis of the X-43 Hypersonic Flight Vehicle," *39th Aerospace Sciences Meeting and Exhibit*, AIAA Paper 2001-0712, 2001.

[3] Guruswamy, G. P., "Time-Accurate Unsteady Aerodynamic and Aeroelastic Calculations of Wings Using Euler Equations," AIAA Paper 88-2281, April 1988.

[4] Rausch, R. D., Batina, J. T., and Yang, H. T. Y., "Three-Dimensional Time-Marching Aeroelastic Analysis Using an Unstructured-Grid Euler Method," *AIAA Journal*, Vol. 31, No. 9, 1993, pp. 1626–1633.

[5] Ricketts, R. H., Noll, T. E., Whitlow, W., and Huttsell, L. J., "An Overview of Aeroelasticity Studies for the National Aero-Space Plane," AIAA Paper 93-1313, April 1993.

[6] Jameson, A., Baker, T. J., and Weatherill, N. P., "Calculation of Inviscid Transonic Flow over a Complete Aircraft," AIAA Paper 86-0103, 1986.

[7] Peraire, J., Peiro, J., Formaggia, L., Morgan, K., and Zienkiewicz, O. C., "Finite Element Euler Computations in Three Dimensions," *International Journal for Numerical Methods in Engineering*, Vol. 26, No. 10, 1988, pp. 2135–2159. doi:10.1002/nme.1620261002

[8] Morgan, K., Peraire, J., and Piero, J., "The Computation of Three Dimensional Flows Using Unstructured Grids," *Computer Methods in Applied Mechanics and Engineering*, Vol. 87, No. 3, 1991, pp. 335–352.

[9] Gupta, K. K., "Development of a Finite Element Aeroelastic Analysis Capability," *Journal of Aircraft*, Vol. 33, No. 5, 1996, pp. 995–1002.

[10] Geuzaine, P., Brown, G., Harris, C., and Farhat, C., "Aeroelastic Dynamic Analysis of a Full F-16 Configuration for Various Flight Conditions," *AIAA Journal*, Vol. 41, No. 3, March 2003, pp. 363–371.

[11] Gupta, K. K., and Bach, C., "Computational Fluid Dynamics-Based Aeroservoelastic Analysis with Hyper-X Applications," *AIAA Journal*, Vol. 45, No. 7, July 2007, pp. 1459–1471. doi:10.2514/1.21992

[12] Gupta, K. K., and Meek, J. L., *Finite Element Multidisciplinary Analysis*, 2nd ed., AIAA Education Series, AIAA, Reston, VA, Sept. 2003.

[13] Cowan, T. J., Arena, A. S., and Gupta, K. K., "Accelerating CFD-based Aeroelastic Prediction Using System Identification," *Journal of Aircraft*, Vol. 38, No. 1, 2001, pp. 81–87.

[14] Lighthill, M. J., "On Displacement Thickness," *Journal of Fluid Mechanics*, Vol. 4, No. 41958, pp. 383–392. doi:10.1017/S0022112058000525

[15] Sankar, L. N., Malone, J. B., and Schuster, D., "Euler Solutions for Transonic Flow past a Fighter Wing," *Journal of Aircraft*, Vol. 24, No. 1, 1987, pp. 10–16.

[16] Gupta, K. K., "STARS: An Integrated General-Purpose Finite Element Structural, Aeroelastic and Aeroservoelastic Analysis Computer Program," NASA TM 4795, May 1997 (Revised Sept. 2006).

[17] Gupta, K. K., Bach, C., Doyle, T., and Hahn, E., "CFD-Based Aeroservoelastic Analysis with Hyper X Applications," *42nd AIAA Aerospace Sciences Meeting and Exhibit*, AIAA Paper 2004-884, Jan. 2004.

[18] Pendleton, E., "Active Aeroelastic Wing," *Technology Horizons*, Vol. 1, No. 2, June 2000, pp. 27–28.

[19] Voracek, D., Pendleton, E., Griffin, K., Reichenbach, E., and Welch, L., "The Active Aeroelastic Wing Flight Research Program," *Symposium on Novel and Emerging Vehicle and Vehicle Technology Concepts (ATV Panel)*, NATO, 2003.

[20] Friedmann, P. P., "Renaissance of Aeroelasticity and its Future," *Journal of Aircraft*, Vol. 36, No. 1, 1999, pp. 105–121.

[21] Livne, E., "Integrated Aeroservoelastic Optimization: Status and Direction," *Journal of Aircraft*, Vol. 36, No. 1, 1999, pp. 122–143.

C. Cesnik
Associate Editor